

## Aging transitions of multimodal oscillators in multilayer networks

Uroš Barać<sup>1</sup>, Matjaž Perc<sup>1,2,3,4</sup> and Marko Gosak<sup>1,5,6,\*</sup><sup>1</sup>Department of Physics, Faculty of Natural Sciences and Mathematics, University of Maribor, Koroška cesta 160, Maribor, Slovenia<sup>2</sup>Community Healthcare Center Dr. Adolf Drošč Maribor, Vošnjakova ulica 2, Maribor, Slovenia<sup>3</sup>Complexity Science Hub Vienna, Josefstädterstrasse 39, Vienna, Austria<sup>4</sup>Department of Physics, Kyung Hee University, 26 Kyungheedaero, Dongdaemun-gu, Seoul, Republic of Korea<sup>5</sup>Institute of Physiology, Faculty of Medicine, University of Maribor, Taborska ulica 8, Maribor, Slovenia<sup>6</sup>Alma Mater Europaea University, Slovenska ulica 17, Maribor, Slovenia

(Received 7 May 2024; accepted 22 August 2024; published 9 September 2024)

When individual oscillators age and become inactive, the collective dynamics of coupled oscillators is often affected as well. Depending on the fraction of inactive oscillators or cascading failures that percolate from crucial information exchange points, the critical shift toward macroscopic inactivity in coupled oscillator networks is known as the aging transition. Here, we study this phenomenon in two overlaid square lattices that together constitute a multilayer network, whereby one layer is populated with slow Poincaré oscillators and the other with fast Rulkov neurons. Moreover, in this multimodal setup, the excitability of fast oscillators is influenced by the phase of slow oscillators that are gradually inactivated toward the aging transition in the fast layer. Through extensive numerical simulations, we find that the progressive inactivation of oscillators in the slow layer nontrivially affects the collective oscillatory activity and the aging transitions in the fast layer. Most counterintuitively, we show that it is possible for the intensity of oscillatory activity in the fast layer to progressively increase to up to 100%, even when up to 60% of units in the slow oscillatory layer are inactivated. We explain our results with a numerical analysis of collective behavior in individual layers, and we discuss their implications for biological systems.

DOI: [10.1103/PhysRevResearch.6.033269](https://doi.org/10.1103/PhysRevResearch.6.033269)

## I. INTRODUCTION

In real-life systems, macroscopic functionality arises from intricate interactions among microscopic components. These systems, ranging from biological networks to technological infrastructures, are vulnerable to both internal failures and external disturbances [1,2]. Coupled systems exhibit diverse responses to various perturbations, notably cascading failures triggered by disruptions in critical information exchange points [3]. Remarkably, the breakdown of such systems presents an array of intriguing behaviors, characterized by distinct phase transitions contingent upon structural or dynamical properties of individual units [4–7]. Within this realm, a specialized subfield investigates the critical shift toward macroscopic inactivity in coupled oscillator networks—the aging transition [8]. The phenomenon, described by Daido and Nakanishi [9,10], explores how the global activity of coupled oscillators deteriorates with an increasing fraction of inactivated elements.

Investigating the dynamical robustness has become highly pertinent to several natural and real-world processes.

Consequently, the aging transition phenomenon has been studied in a variety of contexts [11–13], and in the last decade, efforts have been made to interpret how intricate connectivity patterns influence the dynamical robustness of networked systems [14,15]. It has been identified that the addition of asymmetry [16,17], time delays [18,19], weighted edges [20,21], and repulsive interactions [22] can enhance the dynamical robustness in an aging network. Furthermore, in heavy-tailed networks, it has also been found that the aging transition significantly depends on the order in which nodes become inactive. Despite the established fragility of heterogeneous networks to hub removal [20], it has been observed that, under certain conditions, oscillatory networks can demonstrate pronounced fragility to the deliberate inactivation of low-degree nodes [23–26]. Furthermore, in tandem with the progress in network science, the exploration of aging transitions has expanded to encompass multilayered interactions [27–29]. It has been shown that, while interlayer coupling potentially enhances dynamic survivability, the aging behavior exhibits a nontrivial relationship with regard to both coupling and the strategy of node inactivation [27,28,30,31].

A significant portion of prior studies has focused on paradigmatic Stuart-Landau limit-cycle oscillators. However, research endeavors have also shifted toward coupled excitable units, particularly to study the aging transition in populations of interconnected neurons [21,32–34]. Due to the more complex dynamics of individual units, such systems may exhibit nonintuitive dynamical phenomena, such as enhanced

\*Contact author: [marko.gosak@um.si](mailto:marko.gosak@um.si)

Published by the American Physical Society under the terms of the Creative Commons Attribution 4.0 International license. Further distribution of this work must maintain attribution to the author(s) and the published article's title, journal citation, and DOI.

macroscopic activity due to the inactivation of individual units [35] and, under certain conditions, abrupt transitions to the globally inactive state [36]. Factors like heterogeneity [13,21] and the presence of both mixed attractive and repulsive coupling [37] have been shown by further investigations to influence the dynamical robustness of macroscopic neuronal activity. Moreover, as neurons are known to communicate by different means of communication, such as chemical and electrical synapses [38], the use of multilayer network formalism has become a popular tool to study different aspects of neuronal dynamics [39–42], including their dynamical robustness. Specifically, it has been demonstrated that the presence of additional chemical synaptic coupling [43] or the interlayer ephaptic coupling can enhance dynamical robustness of the multilayered neuronal network [44], while the interlayer memristive synapse coupling has a deteriorating effect [44].

It is imperative to recognize that the oscillatory dynamics of individual units within real-world systems often exhibits a complexity that surpasses the predictions of simple limit-cycle or excitable oscillator models. Namely, many systems demonstrate multimodal activity, characterized by interdependent oscillations occurring on diverse time scales. Such rhythmic activity is usually generated by a complex interplay of different oscillatory subsystems that are driven by different mechanisms but are intertwined with each other. For example, in muscle cells, endocrine cells, and neurons, certain processes occurring on time scales of several minutes—such as rhythmic fluctuations in hormones, metabolites, or specific second messengers—govern the activity of oscillatory processes occurring on shorter time scales, such as calcium or membrane potential oscillations, which have periods on the order of milliseconds to seconds [45–47]. Importantly, in all these cases, coupling between individual cells is required, as it facilitates the synchronous behavior that is essential for normal function [48–51]. Amid the process of pathogenesis, wherein individual cells experience dysfunction, it is possible that only specific subsystems, e.g., the slow ones, are affected by the disease which, however, affects the overall rhythmic activity and function. This served as the main motivation for this paper, in which we aimed to investigate the aging transition in a context of multimodal oscillatory activity. To this end, we constructed a two-layered network model, with each layer representing its own oscillatory subsystem, one slow and the other fast. Within individual layers, oscillators interact with each other, while the interlayer interactions are encompassed by the modulation of the activity of the fast oscillatory layer by the slow oscillators. Employing this multiplex and multimodal model, we proceeded to methodically simulate and examine the impact of oscillator inactivation within the slow oscillatory layer on the macroscopic activity of the fast oscillatory layer. Our numerical analyses unveil intriguing behaviors intricately reliant on the interplay between the fraction of inactivated units and the coupling strengths among both types of oscillators.

## II. COMPUTATIONAL MODEL

In our computational model, we construct a two-dimensional square lattice network with dimensions  $N = L \times L$  nodes, where  $L$  is set to 15, resulting in a grid with 225

nodes in which each node is connected to its four nearest neighbors. This lattice, representing a simplified abstraction of a cellular network, incorporates periodic boundary conditions. Each node can be regarded as a biological cell with inherent oscillatory properties, modeled by two distinct yet interconnected oscillators, one oscillating on a slow time scale and the other on a fast time scale. In this regard, our model is formally presented as a multiplex network, where each layer represents an individual oscillatory component, and the interlayer links signify the modulation of the fast component by the slow oscillatory activity, as indicated in Fig. 1(a). The Poincaré oscillator represents the slow oscillatory rhythms of the cell, such as rhythmic variations in hormone or metabolite concentrations [45–47], while the iterated Rulkov map [52] is used to capture rapid oscillatory activity, such as electrical excitations like those observed in neural, muscle, or endocrine tissue [47,53,54]. The Poincaré oscillator at each node is described by a set of Cartesian differential equations for the variables  $x_i$ ,  $y_i$  as follows:

$$\dot{x}_i = -y_i\omega_i - \gamma x_i(\sqrt{x_i^2 + y_i^2} - A_i) + K_P \sum_{j \in S_i} (x_j - x_i), \quad (1a)$$

$$\dot{y}_i = x_i\omega_i - \gamma y_i(\sqrt{x_i^2 + y_i^2} - A_i) + K_P \sum_{j \in S_i} (y_j - y_i), \quad (1b)$$

where  $\gamma = 1.0$  is the relaxation rate,  $A_i = 1.0$  is the amplitude (for an active set),  $K_P$  the coupling strength between Poincaré oscillators,  $S_i$  denotes the von Neumann neighborhood of node  $i$ , and parameter  $\omega_i$  denotes the intrinsic frequency of the  $i$ th oscillator. To introduce heterogeneity, values of  $\omega_i$  were randomly and uniformly distributed among the oscillators within the range  $\omega_{\text{mean}} \pm 0.15\omega_{\text{mean}}$ , so that the frequencies of the slow oscillatory component varied by  $\pm 15\%$ .

We use the discrete iterative Rulkov map to describe the fast oscillatory activity, as it effectively captures the essence of spiking behavior characteristic of excitable cells [52–54]. The equations are

$$u_i(n+1) = \frac{\alpha_i(n)}{1 + u_i(n)^2} + v_i(n) + D\xi_i(n) + K_R \sum_{j \in S_i} [u_j(n) - u_i(n)], \quad (2a)$$

$$v_i(n+1) = v_i(n) - \sigma u_i(n) - \chi, \quad (2b)$$

where  $n$  is a discrete time step, and  $u_i$  and  $v_i$  are dimensionless variables that resemble the membrane potential and the gating variable, respectively. Here,  $K_R$  is the coupling strength between Rulkov oscillators, and  $D = 0.005$  indicates the strength of Gaussian noise  $\xi$  with mean 0 and variance 1 that accounts for stochasticity in cellular activity. Parameters  $\sigma$  and  $\chi$  were uniform for all oscillators and assigned standard values  $\sigma, \chi = 0.001$ .

Importantly, the parameter  $\alpha_i(n)$  defines the excitability level of the cell, and we introduce interconnectivity between the slow and fast dynamics through modulations of this parameter by the slow oscillatory component. Specifically, we link the amplitude  $x_i$  of the Poincaré oscillator with the excitability level of the Rulkov oscillator  $\alpha_i(n)$  via an

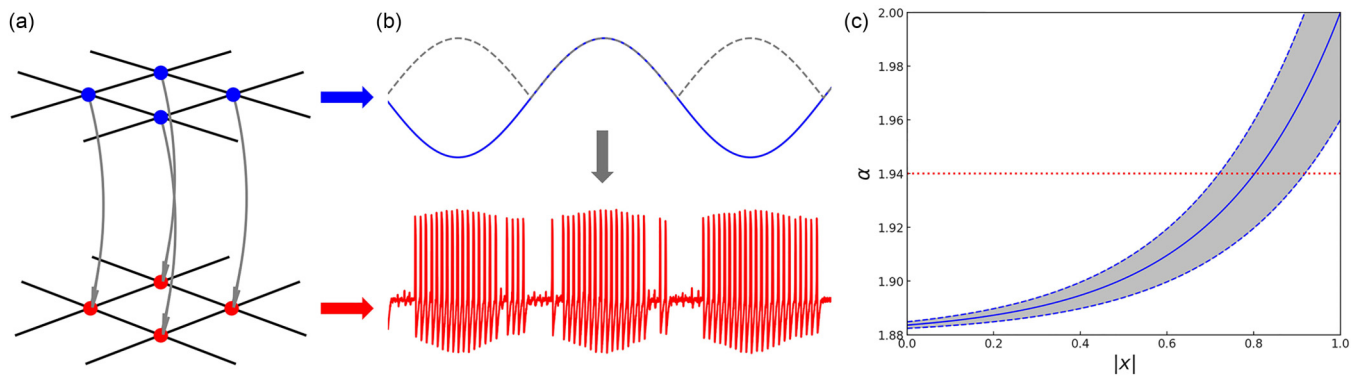


FIG. 1. (a) Schematic representation of two overlaid square lattices indicating the slow (blue nodes) and fast (red nodes) oscillatory components, i.e., a multiplex oscillatory network in which intralayer connections denote coupling between individual oscillators and interlayer connections (represented with gray arrows) indicate the modulation of the fast activity by the slow oscillatory component. (b) Simulated interdependent time traces of a slow component (blue) and a fast component (red). The gray dotted line represents the absolute value of the slow signal which is used to modulate the excitability parameter determining the fast oscillations. (c) The relationship between the absolute amplitude of the Poincaré oscillator and the parameter  $\alpha$  modulating the excitability level of the Rulkov neuron. The shaded area indicates the interindividual variability of the Rulkov oscillator, while the dotted lines indicate the activation threshold of an individual Rulkov neuron.

exponential function as follows:

$$\alpha_i(n) = \alpha_{0,i} \exp[b(|x_i| - 1)] + \alpha_{\text{MIN}}, \quad (3)$$

where the parameter values were set to  $b = 3.5$  and  $\alpha_{\text{MIN}} = 1.88$ . This mechanism ensures that slow oscillatory dynamics can influence the fast activity, a key feature in many physiological processes [45–47]. The resulting interdependent oscillatory behavior is illustrated in Fig. 1(b). Furthermore, to account for heterogeneity in the excitability responses, the parameter  $\alpha$  was randomly distributed so that each  $\alpha_{0,i}$  was selected randomly from a uniform distribution within the interval  $[0.08, 0.16]$ . The relationship between the excitability parameter  $\alpha$  and the absolute amplitude of the slow oscillator  $|x|$  is presented in Fig. 1(c). The modulation of fast oscillations is ensured by the fact that the activation threshold is only exceeded for sufficiently large values of  $|x|$ . The robustness of this effect is further reinforced using a superlinear relationship between  $\alpha$  and  $|x|$ , as in this case, oscillators under normal conditions effectively become inactive and cannot be reactivated at lower values of  $|x|$  even by interactions with potentially active neighbors.

The Poincaré oscillator was numerically solved with Runge-Kutta second-order method and a time step  $dt = 0.05$ , and since the Rulkov model is an iterative map, we set  $dt$  equal to one discrete time step  $n$  in the Rulkov model. The  $\omega_{\text{mean}}$  was then set to 0.003, so that in the time of one Poincaré cycle, the corresponding Rulkov oscillator exhibits  $\sim 15$ – $20$  spikes.

To model deactivation of individual oscillators or cellular aging, we introduce a subset of inactive oscillators into the lattice. By varying the ratio of these inactive elements, the system can be studied across different stages of functionality, from fully active to significantly impaired. The Poincaré oscillators were arranged into two subsets, active and inactive, with their sizes being  $pN$  and  $(p-1)N$ , respectively, where  $p$  is the ratio of inactive oscillators. With increasing the ratio of inactive oscillators, by setting the amplitude  $A_i$  to a negative value, the system then undergoes an aging transition, where the amplitude of the individual Poincaré oscillator decreases

or falls to 0, thereby lowering the maximum excitability and subsequently the oscillation frequency of the corresponding Rulkov oscillator. An individual oscillator is considered inactive if its parameters are changed so that its solution, if the oscillator was uncoupled, becomes a fixed point. We define  $A_i = -1$  if the  $i$ th oscillator is in the inactive set and  $A_i = 1$  if it is in the active set. To quantify the global oscillatory activity of the Poincaré network layer, we compute the average global complex amplitude  $Q = \langle |\sum_{i=1}^N z_i / N| \rangle$ , where  $z_i = x_i + y_i i$ . For the Rulkov network, we calculate the root mean square (RMS) amplitude  $M = \sqrt{\langle (U - \langle U \rangle)^2 \rangle}$  on the variable  $u_i$ , where  $U = \sum_{i=1}^N u_i / N$  is the mean signal. The sums are calculated over all oscillators at a given time  $t$ , and the angle brackets signify a long time average. Additionally, we calculate the average activity of the mean Rulkov oscillations  $T_A$ , which we simply define as the ratio of the time when the average signal  $U$  exceeds a certain threshold value  $\text{th} = -0.75$ . To minimize the effect of any transient phenomena, we ensure that our analysis reflects the steady-state operation of the model, we discard the initial 10 cycles of the Poincaré system.

### III. RESULTS

In Fig. 2, we start by showing the traces of the average signal for both types of oscillators, examining the impacts of varying ratios of inactive oscillators and different coupling strengths on the global amplitude. At low coupling values [Fig. 2(a);  $K_P = 0.0001$  and  $K_R = 0.004$ ], both the fast Rulkov and slow Poincaré layers exhibit desynchronized activity characterized by a low amplitude of the global signal. Here, the system uniformly fails to reach the defined threshold value indicative of active collective dynamics, and the oscillator network remains in a disordered state, with each oscillator effectively acting rather independently from the others. By increasing the coupling in the fast Rulkov layer [Fig. 2(b);  $K_R = 0.007$ ], the global amplitude of Rulkov oscillators increases, while the phase synchronization of Poincaré oscillations remains low. Thus, local synchronization occurs

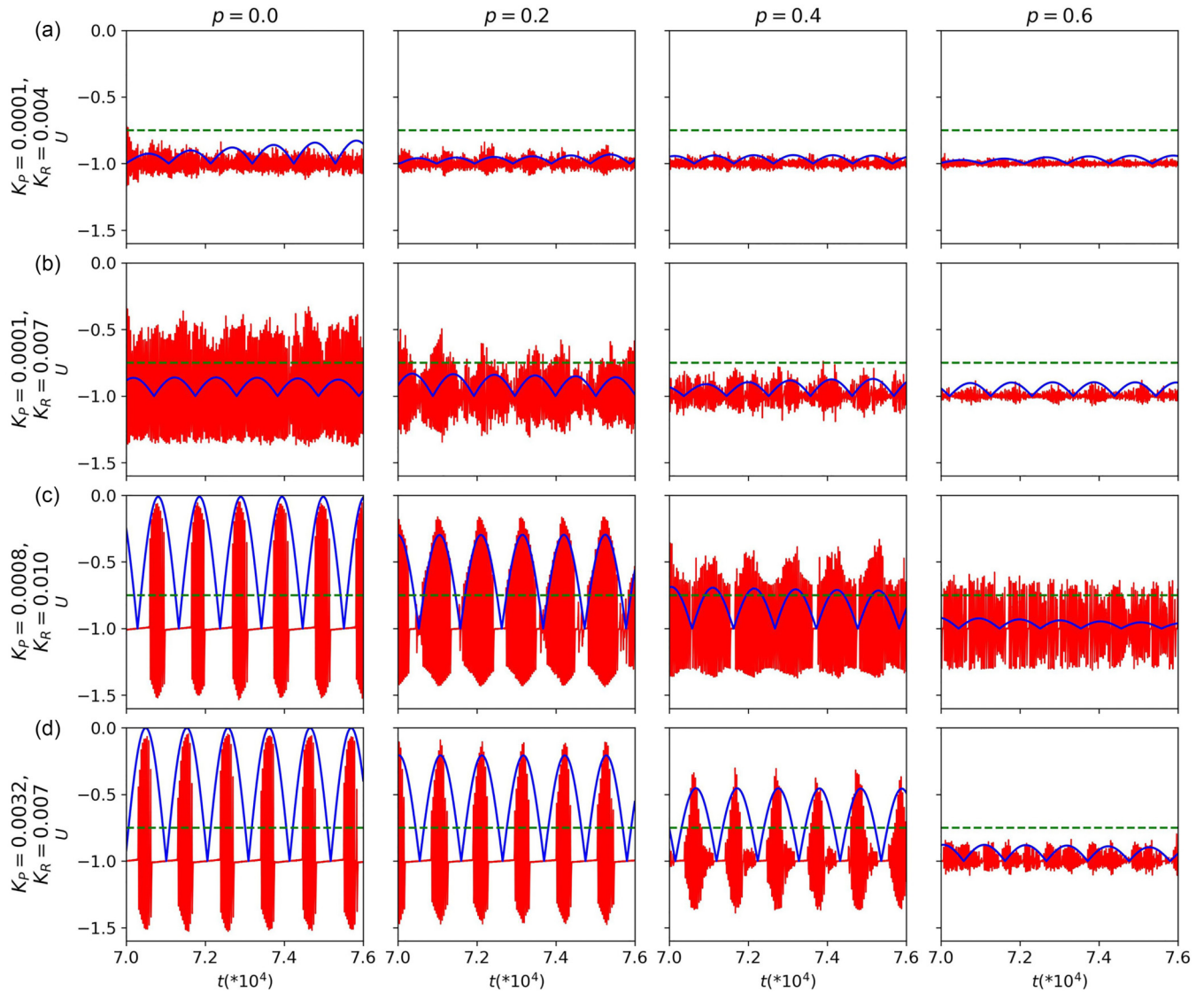


FIG. 2. Traces of the mean signal of the fast Rulkov components  $U$  (red) as a function of time  $t$  for different pairs of coupling strengths  $K_P$  and  $K_R$  and different ratios of inactive oscillators  $p$ : (a) weak coupling in both components, (b) weak coupling in the slow component and intermediate coupling in the fast component, (c) intermediate coupling in both components, and (d) strong coupling in the slow and intermediate coupling in the fast component. Additionally, the trace of the absolute value of the mean signal of the slow Poincaré components  $X$  is plotted over the Rulkov trace (blue). The green dashed line indicates the threshold value  $\text{th} = 0.75$  used for calculating the activity of the average signal of the Rulkov component.

within Rulkov oscillators, but there is no cross-type phase locking between the fast and slow layers, which would result in modulated activity of the fast component. If, however, the coupling among the slow oscillators is increased as well [Fig. 2(c);  $K_P = 0.0008$  and  $K_R = 0.010$ ], we observe distinct narrow phases of fast oscillatory activity characterized by high amplitude, which are in phase with the Poincaré period. Stronger coupling not only induces synchronization within a given oscillator type but also facilitates phase alignment across the different oscillator models, leading to moments of network-wide coherence. Interestingly, as the ratio of inactive oscillators increases, the observed phases of high activity in the Rulkov layer broaden, while the global oscillation amplitude decreases [see Fig. 2(c), second and third panels at  $p = 0.2$  and  $0.4$ ]. The widening of active phases suggests

that the presence of inactive elements within the network can extend the duration of collective activity, albeit with a diminished intensity of the global signal. If the coupling in the Poincaré layer is further increased [Fig. 2(d);  $K_P = 0.0032$  and  $K_R = 0.007$ ], while the effects are less pronounced, the same general trend persists. The Rulkov oscillators display a lower level of distinctiveness in their active phases, with the activity spanning over a slightly wider interval, along with an amplitude reduction as the ratio  $p$  increases [see Fig. 2(d) at  $p = 0.2$ ].

Expanding upon the initial observations presented in Fig. 2, Fig. 3 offers a more comprehensive analysis of the collective dynamics within a network of coupled oscillators. The upper six panels [Fig. 3(a)] provide a color-coded visualization representing the RMS amplitude and activity of the

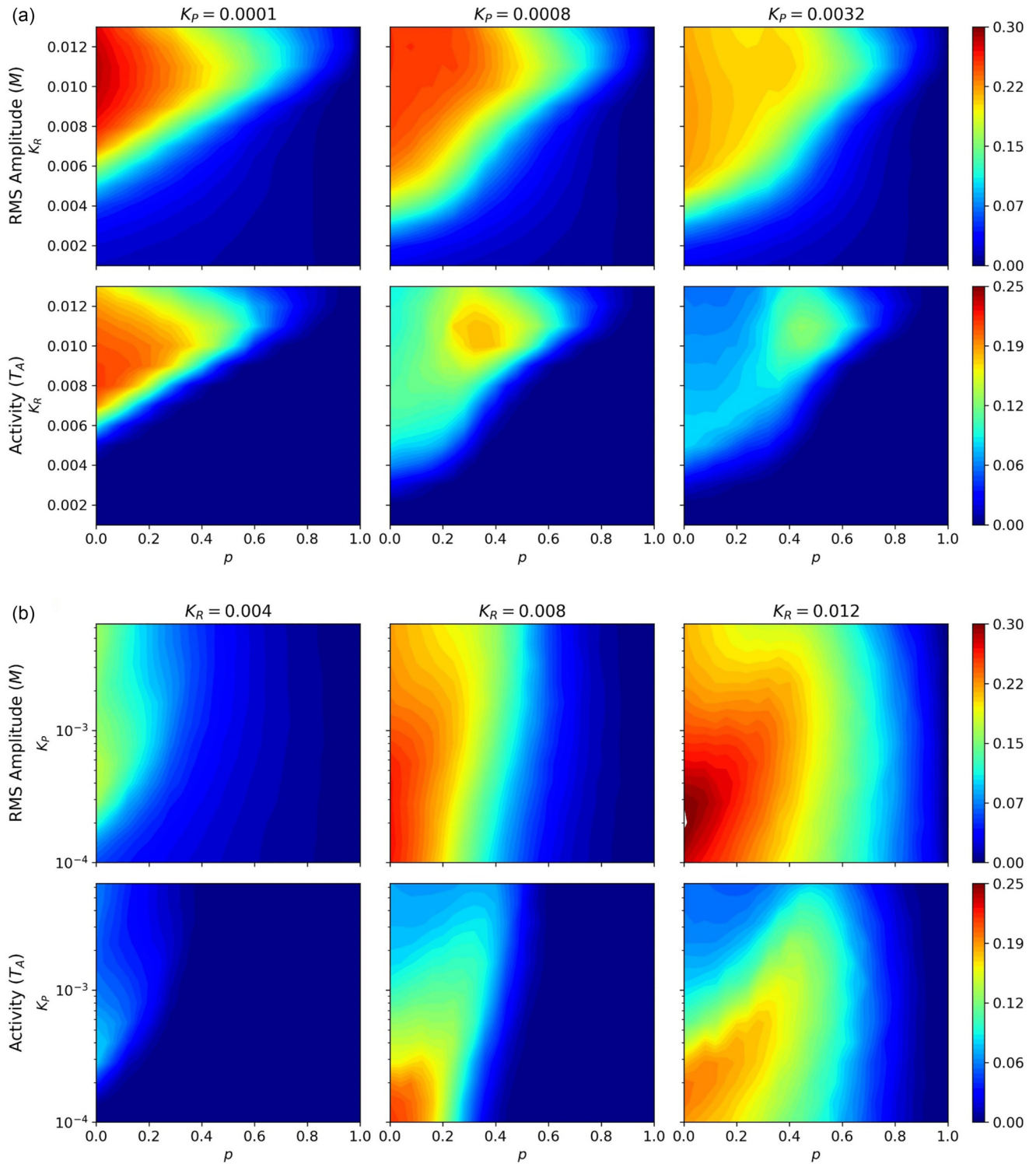


FIG. 3. Color-coded values of the root mean square (RMS) amplitude  $M$  and the activity  $T_A$  of the mean signal of the Rulkov component as a function of the ratio of inactive oscillators  $p$  and either (a) the coupling strength among Poincaré oscillators  $K_R$  where the value of the coupling strength among Poincaré oscillators  $K_P$  is fixed or (b) as a function of  $K_P$  where the coupling among Rulkov oscillators  $K_R$  is fixed. Note that the color scales for the RMS amplitude and the activity are not the same.

Rulkov mean signal as functions of  $p$  and  $K_R$ , with  $K_P$  held constant. Conversely, the lower six panels [Fig. 3(b)] illustrate these dependencies with  $p$  and  $K_P$  varied and  $K_R$  held constant. Evidently, the RMS amplitude gradually decreases with increasing  $p$ , indicating that higher coupling between

the fast oscillators (i.e., increasing values of  $K_R$ ) requires a higher number of inactivated elements to diminish macroscopic activity, except for very high values [ $K_R > 0.01$ ; see upper row in Fig. 3(a)]. In contrast, the relationship between RMS amplitude and the coupling between the slow

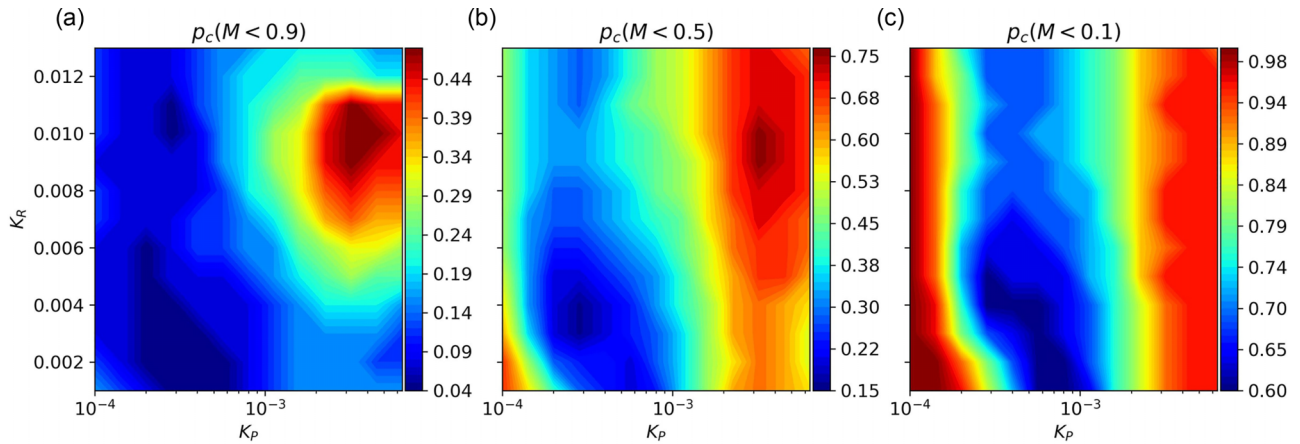


FIG. 4. Color-coded values of the critical value  $p_c$  at which the root mean square (RMS) amplitude of the mean signal of the Rulkov components  $M$  falls below (a) 90%, (b) 50%, and (c) 10% of the starting value [ $M(p=0)$ ], as a function of the coupling strengths between Poincaré oscillators  $K_P$  and Rulkov oscillators  $K_R$ . Notice that each plot has its own color scale.

oscillators is less intuitive and is significantly influenced by the coupling strength between the fast Rulkov oscillators [see upper row in Fig. 3(b)]. Furthermore, analyzing the activity of the oscillators reveals even more interesting dynamical behavior arising from the interplay between the fraction of inactive oscillators and coupling strengths. The second rows in Figs. 3(a) and 3(b) display color-coded values of relative active time  $T_A$  as a function of inactivated elements  $p$  and coupling strengths. In principle, the activity is higher and persists for higher values of inactivated elements when the coupling in the fast layer is stronger. Conversely, stronger coupling in the slow layers has the opposite effect, leading to lower activity. Notably, for intermediate to high values of both  $K_P$  and  $K_R$ , we observe a significant increase in the activity of oscillators with higher values of inactivated elements [see the second and third columns in Figs. 3(a) and 3(b)]. Maxima in activity can occur with up to 60% inactivated elements, resulting in a relative increase of up to 100% compared with the initial activity without inactivated elements. The non-monotonic response suggests a resonantlike behavior in the oscillatory network, where a specific proportion of inactivity within the coupled system may enhance conditions for collective excitation, which is further addressed in continuation. Notably, in our analysis, we used the relative active time of the global signal  $T_A$  as an indicator of activity. This metric is frequently used in cellular physiology because it represents the proportion of time cells spend in the active phase (i.e., the relative proportion of time they are depolarized). Given that the length of individual global oscillations changes minimally, the frequency of oscillations could, in principle, also serve as a measure of activity and would yield qualitatively similar results.

In Fig. 4, we visualize the robustness of the oscillator network in further detail by analyzing how the interplay between the coupling strengths in both network layers affect the critical value of the inactivity ratio  $p$  ( $p_c$ ) at which the RMS amplitude of the mean signal  $M$  of the Rulkov component drops below certain percentages of its initial value [i.e., compared with  $M(p=0)$ , without inactivated elements]. Figure 4(a) provides a heat map indicating the critical value  $p_c$  where  $M$  falls below 90% of its initial value. For interme-

diante values of  $K_R$  and for high values of  $K_P$ , this threshold is reached by the highest fraction of inactivated elements ( $p_c \approx 0.45$ ), suggesting a stronger robustness against inactivity in this parameter regime. Figure 4(b) reveals that the RMS amplitude remains above half of its initial value, where principally, again, intermediate coupling in the fast layer and strong coupling in the slow layer represent the most resilient setup. In this regime, a less distinct peak is observed at  $\sim 75\%$  of inactivated oscillators. Finally, Fig. 4(c) visualizes when in the coupling parameter space the macroscopic activity falls below 10% of the initial value. We can observe that, in the case of weak coupling among Poincaré oscillators, the activity remains above this threshold for large fractions of inactive elements. This is because weak interactions of macroscopic oscillations prevent them from being completely suppressed, even with a fraction of  $p > 90\%$ . On the other hand, strong coupling in the slow layer also requires a large fraction of inactive oscillators to almost completely suppress activity, i.e., to cause a drop below 10% of the initial value. However, the system loses global oscillatory activity most rapidly at intermediate coupling values in the slow component. These observations are relatively independent of the strength of coupling among Rulkov oscillators.

To examine in more detail how the phase of slow oscillations modulates the fast ones and how this reflects on the overall activity, we show in Fig. 5 a polar representation that illustrates the relationship between the faster Rulkov component and the slower Poincaré component under various network conditions. This polar graph demonstrates the average activity of the Rulkov signal, categorized by segmented phases of the period of the Poincaré signal. Each phase of the slow Poincaré signal is divided into 12 equal segments represented by the angle, while the radial distance from the origin correlates to the average activity of the Rulkov signal within each phase segment. The diagram incorporates various colored lines to depict the system under different proportions of inactive oscillators  $p$ , paralleling the conditions investigated in Figs. 2 and 5. The close-to-zero values for low  $K_P$  and  $K_R$  values [Fig. 5(a)] indicate a lack of well-defined global activity due to the absence of interactions and synchronous behavior. When the coupling within the fast

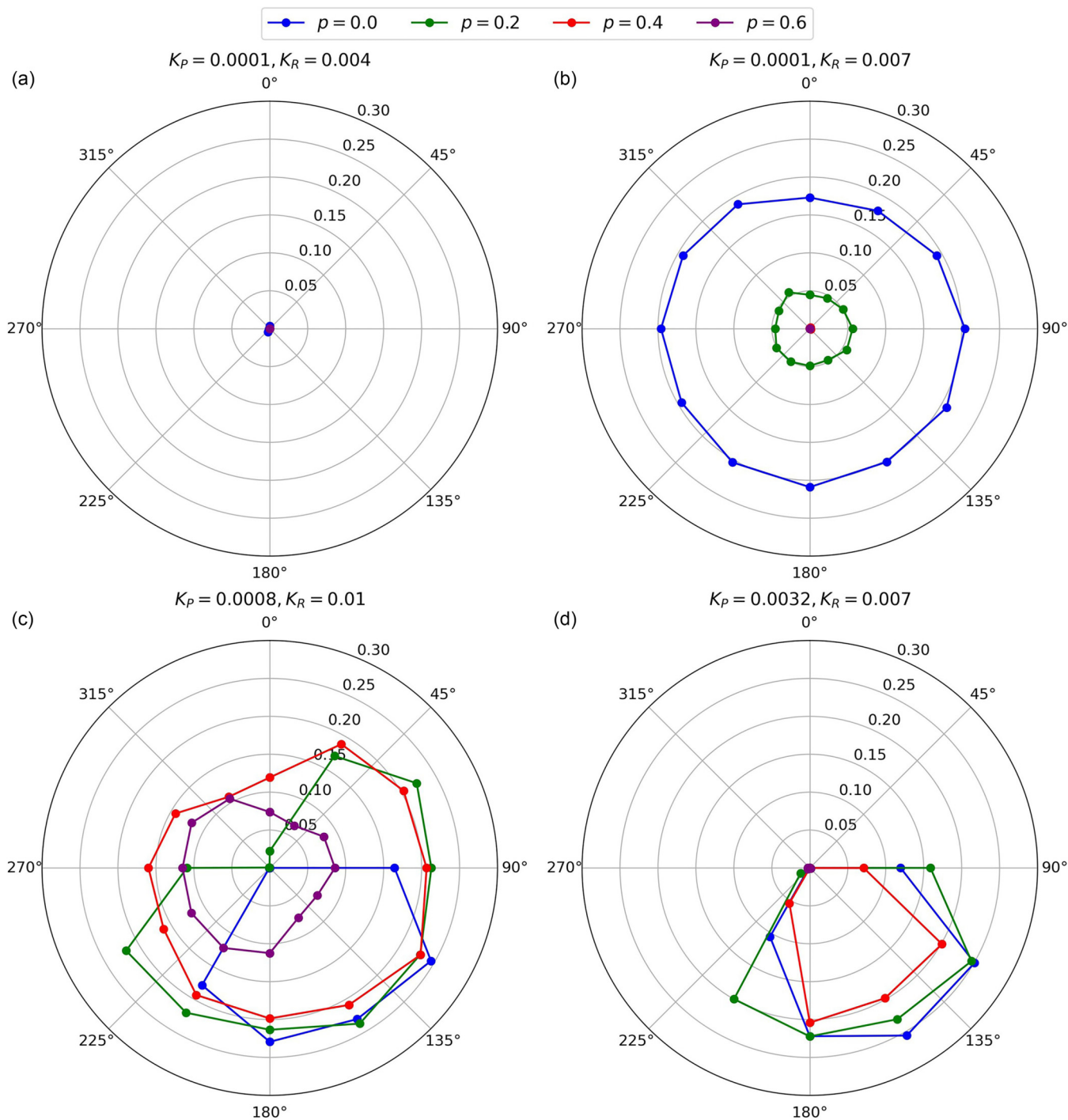


FIG. 5. Polar representation of average activity of the mean fast Rulkov signal over segmented phases of the period of the mean slow Poincaré signal, for different ratios of inactive oscillators  $p$  and distinct coupling strengths between Poincaré and Rulkov oscillators  $K_p$  and  $K_R$  (note that the values are the same as in Fig. 2): (a) weak coupling in both components, (b) weak coupling in the slow component and intermediate coupling in the fast component, (c) intermediate coupling in both components, and (d) strong coupling in the slow and intermediate coupling in the fast component. In all panels, the angle denotes the phase of the slow period divided into 12 equal segments. Radial distance from the origin indicates the average activity within each phase segment. The various colored lines represent different proportions of inactive oscillators in the system ( $p = 0.0, 0.2, 0.4,$  and  $0.6$ ).

network layer is increased while the interactions within the slow layer remain small [Fig. 5(b)], the activity becomes well pronounced. However, it is completely independent of the phase of the Poincaré oscillator and diminishes completely even for  $p = 0.4$ . If the coupling constant  $K_p$  is increased

as well [Fig. 5(c)], the frequency variation of Rulkov oscillations shows a significant dependence on the Poincaré phase. Importantly, an increase in the fraction of inactivated elements results in a loss of this modulation, leading to the Rulkov oscillations becoming rather independent of the

slowly modulating phase. If, however, we move to the very strong coupling regime [Fig. 5(d)], the distribution of activity in the fast layer is highly dependent on the slow component as well, but in this case, the dependence holds even as the proportion of inactive elements increases. These results help to understand the before-mentioned nontrivial dependence of activity on the proportion of inactive elements, which was rather unintuitively found to increase for moderate coupling values between both oscillatory components. Thus, from the results in Fig. 5, we can see that this is due to the loss of modulation capability of the fast component by the slow one as  $p > 0$ , leading to activity spreading across the entire phase and resulting in an increase in activity at the global level.

To gain deeper insights into the nontrivial behavior described earlier, we further examine the dynamics of individual oscillatory units. Figure 6 presents the spatial distribution of individual Rulkov oscillators within a square lattice and a color-coded representation of their activity. This visualization highlights the effects of varying ratios of inactive oscillators and the coupling strengths between Poincaré and Rulkov oscillators. The intensity of color in each element represents the activity of the individual Rulkov oscillator, with the shapes denoting the activity status of the corresponding Poincaré oscillator: circles for active and crosses for inactive. Each lattice configuration is accompanied by the calculated average correlation ( $\text{corr}$ ) between all active Poincaré oscillators. These results allow for an intuitive grasp of the interplay between oscillator activity, coupling strength, and fraction of inactivated oscillators.

First, it is evident that a reduced correlation among the Poincaré oscillators does not necessarily result in diminished activity of the Rulkov oscillators. Instead, for  $p > 0$  and for high enough values of  $K_P$  and  $K_R$ , Rulkov oscillators (even the ones in the inactive set) exhibit higher activity compared with scenarios where all oscillators are active [see Fig. 6(c) for  $p > 0$  and Fig. 6(d) for  $p = 0.2$  and  $0.4$ ]. This counterintuitive outcome is reminiscent of the findings presented in Figs. 5(c) and 5(d), and it can be attributed to the loss of radial dependence of the activity of the fast component on the slow phase. Secondly, we can also observe that the activity of inactive elements does not diminish, even though the amplitude of the Poincaré oscillations is zero, and therefore, a solitary Rulkov oscillator would not be able to surpass the activation threshold. However, coupling within the lattice enables the propagation of excitation waves, which can spread from active oscillators to areas of inactivity. As shown in Fig. 6, this is most pronounced when the cluster of inactive elements is small and surrounded by a larger number of active ones. Additional insight into the wave dynamics within the fast oscillatory layer is provided by Videos S1–S3 in the Supplemental Material [55], illustrating the propagation of waves in various scenarios. In Videos S1 and S2 in the Supplemental Material [55], using parameter settings of  $K_P = 0.0008$  and  $K_R = 0.01$  (i.e., intermediate coupling degree), wave propagation is observed for  $p = 0$  as well as for  $p = 0.4$ . In the former case, fast-moving waves characterize the spatiotemporal activity, leading to synchronous participation of the entire network in wave propagation. This reflects a high level of collective behavior that is also strongly influenced by the phase of slow oscillations. In contrast, the latter case shows slower waves

that transverse inactive elements, with their abundance weakly dependent on slow activity. This behavior corresponds to the increased activity observed at  $p > 0$  in Figs. 3 and 6(c), notable only with high enough coupling strengths. On the other hand, Video S3 in the Supplemental Material [55] showcases spatiotemporal activity for lower coupling strengths ( $K_P = 0.0001$ ,  $K_R = 0.007$ ) and  $p = 0.4$ . Here, waves are slower and more localized, with their abundance weakly dependent of slow oscillatory dynamics. Notably, excitation waves rarely propagate across inactivated elements, acting as barriers to signal propagation.

#### IV. DISCUSSION

The aging transition represents an intriguing dynamical phenomenon observed in networked oscillatory systems, marked by the cessation of macroscopic oscillations resulting from the malfunction of individual units. The investigation of aging within coupled dynamical networks holds not only theoretical appeal but also significant practical relevance, offering valuable insights into the properties and functions of real complex systems as well as their robustness and fragility. In this paper, our aim was to broaden the understanding of the aging transition phenomenon to encompass a network of multimodal oscillators. To this end, we devised a model structured as a two-layered multiplex network. Each layer represents a distinct oscillatory subsystem: one characterized by slow oscillations and the other by fast oscillations. Most importantly, the interactions between oscillators are not confined solely to within the same layer but also encompass interlayer interactions, so that the activity of fast oscillators is influenced by the phase of slow oscillators. In the context of aging transition, we then progressively inactivated only the oscillators in the slow layer and examined the impact this had on the fast oscillatory dynamics.

Such an arrangement can be applied to describe various biological systems, particularly those where rhythmic activity is characterized by oscillations on different time scales and results from interactions among many units. For example, in pancreatic islets of Langerhans, insulin-secreting  $\beta$  cells are coupled via different communication pathways to work in synchrony, and the activity of each  $\beta$  cell is characterized by tightly coupled membrane potential and intracellular calcium concentration dynamics that are intertwined with oscillations in metabolism that occur on an order of magnitude lower time scale [56]. The resulting dynamics is multimodal and originates from networked feedback interactions of various oscillatory subsystems [57]. Most importantly, the oscillatory activities are interdependent, so that the fast oscillations are governed by the phase of slow oscillations [47,53,58]. Likewise, neural population activity arises from intricate networked interactions and exhibits a spectrum of frequencies. For instance, it has been shown that, in spinal neurons, rhythmic variations of cyclic adenosine monophosphate occurring on time scales of minutes modulate the spiking activity occurring on a shorter time scale [45]. Along similar lines, phase-locked neuronal firing driven by slow-scale oscillations has also been reported in pyramidal neurons [46], neurons in the subcortical visual system [59], and for the hippocampal neural network whose activity is guided by slow modulatory

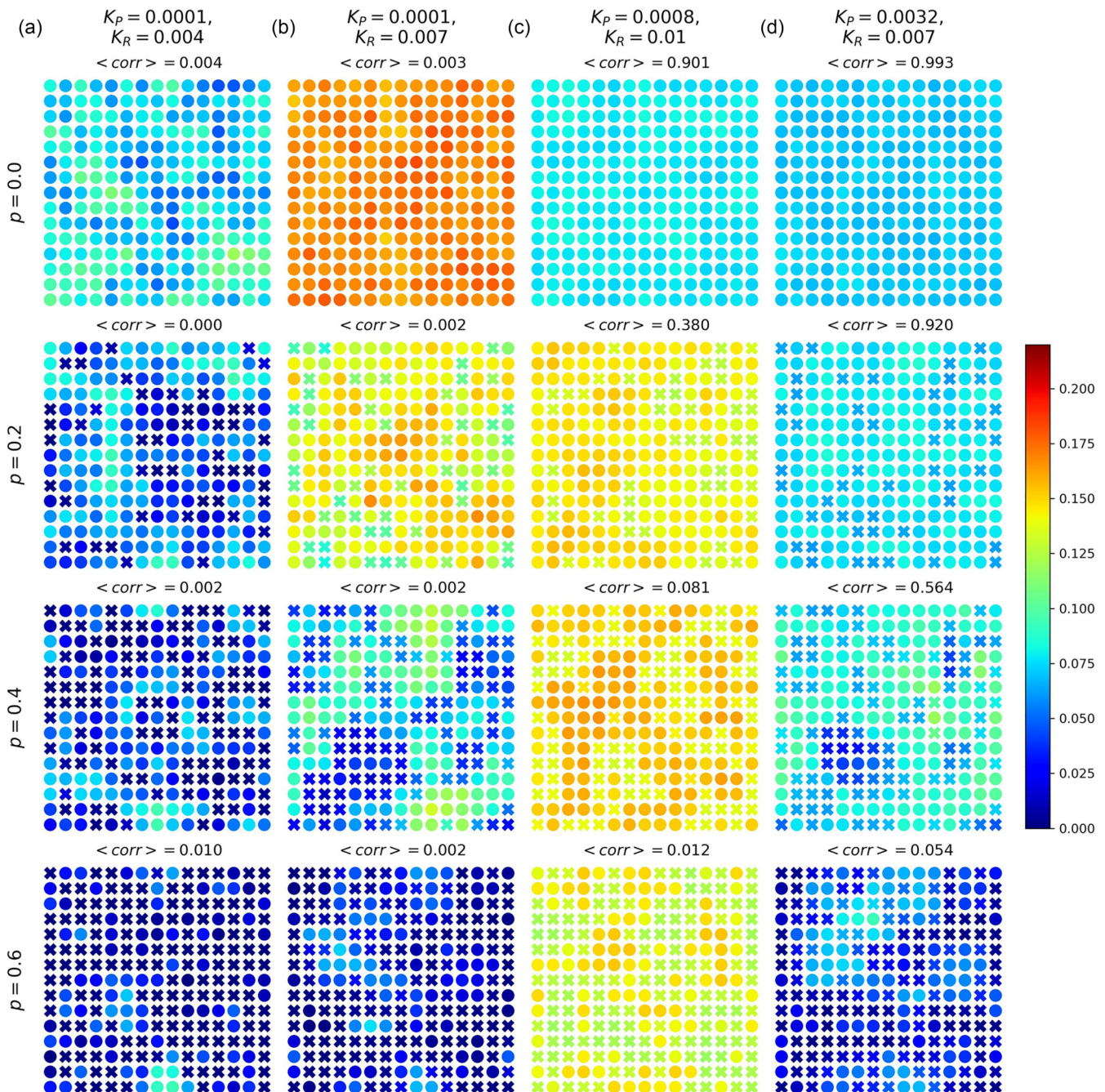


FIG. 6. Spatial and color-coded representation of oscillator activity and position within a square lattice of individual Rulkov oscillators for varying inactive oscillator ratios  $p$  and coupling strengths between Poincaré and Rulkov oscillators  $K_P$  and  $K_R$ : (a) weak coupling in both components, (b) weak coupling in the slow component and intermediate coupling in the fast component, (c) intermediate coupling in both components, and (d) strong coupling in the slow and intermediate coupling in the fast component. Note that the values are the same as in Figs. 2 and 5. Color intensity indicates the activity of individual Rulkov oscillators. The shapes denote whether the corresponding Poincaré oscillator is in the active (circles) or inactive set (crosses). The calculated average correlation  $\langle \text{corr} \rangle$  between Poincaré oscillators is displayed for each scenario where only the oscillators in the active subset were considered, as the inactive oscillators do not exhibit any oscillations.

astrocytic signaling [60]. In this regard, the collective neural activity can also be understood as a multilayered network of multimodal oscillatory units, consisting of intertwined oscillatory subsystems [61]. The fact that, in this paper, we targeted only the slow oscillators reflects a scenario where pathogenesis targets specific intracellular processes regulating slow oscillations, which in turn also affects the collective rhythmic

activity of the fast component responsible for ensuring physiological functions.

In this paper, we have shown that the progressive inactivation of oscillators in the slow layer nontrivially affects the oscillatory activity in the fast layer and that the nature of the aging transition is nontrivially dependent on the strength of coupling between oscillators within individual layers. Perhaps

the most striking observation pertains to the finding that, for moderate coupling strengths, the intensity of oscillatory activity progressively increases with the increase in inactivated oscillators, even to up to 60% of inactivated units. We have found that this is due to the loss of synchrony among oscillators in the slow layer, leading to the loss of modulation of fast oscillations by the underlying slow oscillatory component as well as due to the propagation of excitation waves that can, under certain conditions, encompass inactivated elements as well. This manifests as both increased overall activity and the presence of oscillations during periods when they should not be present. In other words, under specific conditions, the distribution of activity patterns broadens [see Fig. 5(c)], as the oscillations of the fast component become more numerous on the global level. These conditions refer to an intermediate coupling strength in both the slow and fast layers, which leads to partial synchronization and the propagation of excitation waves as well as a codependent influence on the global spatiotemporal oscillatory activity. These conditions can, in principle, also be satisfied with a slightly modified model. In this paper, we conducted the numerical investigation on a square lattice, but we obtain qualitatively similar results if we use a triangular lattice or a random geometric network as the basic coupling scheme (see Videos S4–S7 in the Supplemental Material [55]). Notably, in all these coupling schemes, interactions are limited to neighboring oscillators which, combined with heterogeneity, prevent the emergence of a globally synchronized state. However, all these networks support the propagation of excitation waves and can thus serve as models for biological tissues and, most importantly, exhibit an increased activity profile for intermediate coupling strength as the number of inactivated elements increases. Moreover, to make our model more realistic in describing neuronal activity, we incorporated a noise term, reflecting the stochastic nature of realistic neural systems. This also ensures a relatively broad range of the excitability parameter  $\alpha$  [Fig. 1(c)], within which wave propagation occurs, with the frequency of these waves also depending on the specific value of this parameter (see Ref. [54] for further insight). It is worth noting that the

presence of a stochastic term is not a necessary condition for obtaining the results, as excitation waves can be produced in a similar manner even in the absence of noise. However, in this case, the relationship between excitability parameter  $\alpha$  and the amplitude of the slow component [Eq. (3)] must be adjusted, specifically by increasing  $\alpha_{\text{MIN}}$  from 1.88 to 1.90 due to the higher activation threshold resulting from the absence of the stochastic component. Videos S8 and S9 in the Supplemental Material [55] demonstrate animations in the noise-free scenario, where again a broadening of activity is observed at  $p > 0$ , like in the original model.

Notably, behavior described above can also be understood in the context of various pathological conditions. For example, in the early stages of diabetes, pancreatic  $\beta$  cells often exhibit increased sensitivity and activity, which results from impaired cellular metabolism that can be linked to the loss of slow metabolic oscillatory activity [62]. Furthermore, increased activity can be noted in the early phases of several types of neurodegenerative diseases, where the increased neuronal firing is associated with compensatory mechanisms which, however, can also contribute to disease progression and symptoms [63–65]. As such abnormalities in biological network dynamics could cause instability and contribute to disease progression, it is important to understand the underlying mechanisms for developing targeted treatments, especially because suppressing abnormal oscillatory patterns might effectively mitigate or prevent the onset of irreversible damage [66]. Hopefully, our findings, albeit solely on the theoretical level, shed light on the complex interplay between specific oscillatory components, the collective activity within biological networks, and how these rhythms can be perturbed during pathogenesis.

#### ACKNOWLEDGMENTS

The authors acknowledge the support by the Slovenian Research and Innovation Agency (Research Core Funding No. P1-0403, No. P3-0396, and No. I0-0029 and Research Projects No. J3-3077).

- [1] R. Albert, H. Jeong, and A. L. Barabási, Error and attack tolerance of complex networks, *Nature (London)* **406**, 378 (2000).
- [2] O. Artime, M. Grassia, M. De Domenico, J. P. Gleeson, H. A. Makse, G. Mangioni, M. Perc, and F. Radicchi, Robustness and resilience of complex networks, *Nat. Rev. Phys.* **6**, 114 (2024).
- [3] A. E. Motter and Y.-C. Lai, Cascade-based attacks on complex networks, *Phys. Rev. E* **66**, 065102(R) (2002).
- [4] A. Bashan, Y. Berezin, S. V. Buldyrev, and S. Havlin, The extreme vulnerability of interdependent spatially embedded networks, *Nat. Phys.* **9**, 667 (2013).
- [5] F. Radicchi and G. Bianconi, Redundant interdependencies boost the robustness of multiplex networks, *Phys. Rev. X* **7**, 011013 (2017).
- [6] A. Arenas, A. Díaz-Guilera, J. Kurths, Y. Moreno, and C. Zhou, Synchronization in complex networks, *Phys. Rep.* **469**, 93 (2008).
- [7] K. P. O’Keeffe, H. Hong, and S. H. Strogatz, Oscillators that sync and swarm, *Nat. Commun.* **8**, 1504 (2017).
- [8] W. Zou, D. V. Senthilkumar, M. Zhan, and J. Kurths, Quenching, aging, and reviving in coupled dynamical networks, *Phys. Rep.* **931**, 1 (2021).
- [9] H. Daido and K. Nakanishi, Aging and clustering in globally coupled oscillators, *Phys. Rev. E* **75**, 056206 (2007).
- [10] H. Daido and K. Nakanishi, Aging transition and universal scaling in oscillator networks, *Phys. Rev. Lett.* **93**, 104101 (2004).
- [11] G. Tanaka, Y. Okada, and K. Aihara, Phase transitions in mixed populations composed of two types of self-oscillatory elements with different periods, *Phys. Rev. E* **82**, 035202(R) (2010).
- [12] H. Daido, Dynamics of a large ring of coupled active and inactive oscillators, *Phys. Rev. E* **83**, 026209 (2011).
- [13] G. Tanaka, K. Morino, H. Daido, and K. Aihara, Dynamical robustness of coupled heterogeneous oscillators, *Phys. Rev. E* **89**, 052906 (2014).
- [14] T. Sasai, K. Morino, G. Tanaka, J. A. Almendral, and K. Aihara, Robustness of oscillatory behavior in correlated networks, *PLoS One* **10**, e0123722 (2015).

- [15] S. Majhi, Dynamical robustness of complex networks subject to long-range connectivity, *Proc. R. Soc. A* **478**, 20210953 (2022).
- [16] Y. Liu, W. Zou, M. Zhan, J. Duan, and J. Kurths, Enhancing dynamical robustness in aging networks of coupled nonlinear oscillators, *Europhys. Lett.* **114**, 40004 (2016).
- [17] S. Kundu, S. Majhi, P. Karmakar, D. Ghosh, and B. Rakshit, Augmentation of dynamical persistence in networks through asymmetric interaction, *Europhys. Lett.* **123**, 30001 (2018).
- [18] B. Thakur, D. Sharma, and A. Sen, Time-delay effects on the aging transition in a population of coupled oscillators, *Phys. Rev. E* **90**, 042904 (2014).
- [19] K. Sathiyadevi, D. Premraj, T. Banerjee, Z. Zheng, and M. Lakshmanan, Aging transition under discrete time-dependent coupling: Restoring rhythmicity from aging, *Chaos Solit. Fractals* **157**, 111944 (2022).
- [20] Z. He, S. Liu, and M. Zhan, Dynamical robustness analysis of weighted complex networks, *Physica A* **392**, 4181 (2013).
- [21] A. Ray, S. Kundu, and D. Ghosh, Aging transition in weighted homogeneous and heterogeneous networks, *Europhys. Lett.* **128**, 40002 (2019).
- [22] A. Sharma and B. Rakshit, Dynamical robustness in presence of attractive-repulsive interactions, *Chaos Solit. Fractals* **156**, 111823 (2022).
- [23] G. Tanaka, K. Morino, and K. Aihara, Dynamical robustness in complex networks: The crucial role of low-degree nodes, *Sci. Rep.* **2**, 232 (2012).
- [24] W. Huang, X. Zhang, X. Hu, Y. Zou, Z. Liu, and S. Guan, Variation of critical point of aging transition in a networked oscillators system, *Chaos* **24**, 023122 (2014).
- [25] T. Yuan, K. Aihara, and G. Tanaka, Robustness and fragility in coupled oscillator networks under targeted attacks, *Phys. Rev. E* **95**, 012315 (2017).
- [26] U. Barać, M. Perc, and M. Gosak, Determinants of collective failure in excitable networks, *Chaos* **33**, 043120 (2023).
- [27] K. Morino, G. Tanaka, and K. Aihara, Robustness of multilayer oscillator networks, *Phys. Rev. E* **83**, 056208 (2011).
- [28] X.-F. Song and W.-Y. Wang, Target inactivation and recovery in two-layer networks, *Chin. Phys. Lett.* **32**, 110502 (2015).
- [29] S. Kundu, S. Majhi, and D. Ghosh, Persistence in multilayer ecological network consisting of harvested patches, *Chaos* **31**, 033154 (2021).
- [30] Y. Wang, Z. Sun, H. Zhang, S. Liu, and W. Xu, Dynamic survivability of two-layer networks with different topologies, *Eur. Phys. J. Plus* **139**, 94 (2024).
- [31] Y. Wang, Z. Sun, H. Zhang, Y. Zhou, S. Liu, and W. Xu, Dynamic survivability of two-layer networks: The role of interlayer coupling, *Chaos Solit. Fractals* **180**, 114571 (2024).
- [32] D. Pazó and E. Montbrió, Universal behavior in populations composed of excitable and self-oscillatory elements, *Phys. Rev. E* **73**, 055202(R) (2006).
- [33] H. Daido and K. Nishio, Bifurcation and scaling at the aging transition boundary in globally coupled excitable and oscillatory units, *Phys. Rev. E* **93**, 052226 (2016).
- [34] I. Ratas and K. Pyragas, Macroscopic self-oscillations and aging transition in a network of synaptically coupled quadratic integrate-and-fire neurons, *Phys. Rev. E* **94**, 032215 (2016).
- [35] I. Ratas and K. Pyragas, Macroscopic oscillations of a quadratic integrate-and-fire neuron network with global distributed-delay coupling, *Phys. Rev. E* **98**, 052224 (2018).
- [36] D. Biswas and S. Gupta, Ageing transitions in a network of Rulkov neurons, *Sci. Rep.* **12**, 433 (2022).
- [37] S. Dixit, P. A. M., and M. D. Shrimali, Aging in global networks with competing attractive-repulsive interaction, *Chaos* **30**, 123112 (2020).
- [38] A. E. Pereda, Electrical synapses and their functional interactions with chemical synapses, *Nat. Rev. Neurosci.* **15**, 250 (2014).
- [39] V. Nicosia, P. S. Skardal, A. Arenas, and V. Latora, Collective phenomena emerging from the interactions between dynamical processes in multiplex networks, *Phys. Rev. Lett.* **118**, 138302 (2017).
- [40] S. Majhi, B. K. Bera, D. Ghosh, and M. Perc, Chimera states in neuronal networks: A review, *Phys. Life. Rev.* **28**, 100 (2019).
- [41] S. Rakshit, B. K. Bera, and D. Ghosh, Synchronization in a temporal multiplex neuronal hypernetwork, *Phys. Rev. E* **98**, 032305 (2018).
- [42] D. Ristič and M. Gosak, Interlayer connectivity affects the coherence resonance and population activity patterns in two-layered networks of excitatory and inhibitory neurons, *Front. Comput. Neurosci.* **16**, 885720 (2022).
- [43] S. Kundu, S. Majhi, and D. Ghosh, Chemical synaptic multiplexing enhances rhythmicity in neuronal networks, *Nonlinear Dyn.* **98**, 1659 (2019).
- [44] Y. Liu, Z. Sun, X. Yang, and W. Xu, Analysis of dynamical robustness of multilayer neuronal networks with inter-layer ephaptic coupling at different scales, *Appl. Math. Modell.* **112**, 156 (2022).
- [45] Y. V. Gorbunova and N. C. Spitzer, Dynamic interactions of cyclic AMP transients and spontaneous Ca<sup>2+</sup> spikes, *Nature (London)* **418**, 93 (2002).
- [46] A. Navas-Olive, M. Valero, T. Jurado-Parras, A. de Salas-Quiroga, R. G. Averkin, G. Gambino, E. Cid, and L. M. de la Prida, Multimodal determinants of phase-locked dynamics across deep-superficial hippocampal sublayers during theta oscillations, *Nat. Commun.* **11**, 2217 (2020).
- [47] J. Zmazek, M. S. Klemen, R. Markovič, J. Dolenšek, M. Marhl, A. Stožer, and M. Gosak, Assessing different temporal scales of calcium dynamics in networks of beta cell populations, *Front. Physiol.* **12**, 612233 (2021).
- [48] R. E. Haddock and C. E. Hill, Rhythmicity in arterial smooth muscle, *J. Physiol.* **566**, 645 (2005).
- [49] G. D. Potter, T. A. Byrd, A. Mugler, and B. Sun, Communication shapes sensory response in multicellular networks, *Proc. Natl. Acad. Sci. USA* **113**, 10334 (2016).
- [50] R. K. P. Benninger and V. Kravets, The physiological role of  $\beta$ -cell heterogeneity in pancreatic islet function, *Nat. Rev. Endocrinol.* **18**, 9 (2021).
- [51] G. Li, R. LeFebvre, A. Starman, P. Chappell, A. Mugler, and B. Sun, Temporal signals drive the emergence of multicellular information networks, *Proc. Natl. Acad. Sci. USA* **119**, e2202204119 (2022).
- [52] N. F. Rulkov, Modeling of spiking-bursting neural behavior using two-dimensional map, *Phys. Rev. E* **65**, 041922 (2002).
- [53] M. Šterk, U. Barać, A. Stožer, and M. Gosak, Both electrical and metabolic coupling shape the collective multimodal activity and functional connectivity patterns in beta cell collectives: A computational model perspective, *Phys. Rev. E* **108**, 054409 (2023).

- [54] A. Stožer, R. Markovič, J. Dolenšek, M. Perc, M. Marhl, M. S. Rupnik, and M. Gosak, Heterogeneity and delayed activation as hallmarks of self-organization and criticality in excitable tissue, *Front. Physiol.* **10**, 869 (2019).
- [55] See Supplemental Material at <http://link.aps.org/supplemental/10.1103/PhysRevResearch.6.033269> for Videos S1–S3 of animations showing spatiotemporal activity of the fast layer at different parameter values (on a square lattice); Videos S4 and S5 of animations showing spatiotemporal activity of the fast layer at different parameter values (on a triangular lattice); Videos S6 and S7 of animations showing spatiotemporal activity of the fast layer at different parameter values (on a random geometric network); and Videos S8 and S9 of animations showing spatiotemporal activity of the fast layer at different parameter values for the noise-free model (on a square lattice). Note that the parameter  $\alpha_{\text{MIN}}$  was increased in this case from 1.88 to 1.90 to facilitate the presence of excitation waves in the absence noise.
- [56] R. Bertram, A. Sherman, and L. S. Satin, Electrical bursting, calcium oscillations, and synchronization of pancreatic islets, in *The Islets of Langerhans*, edited by M. Islam (Springer, Dordrecht, 2010), pp. 261–279.
- [57] I. Marinelli, P. A. Fletcher, A. S. Sherman, L. S. Satin, and R. Bertram, Symbiosis of electrical and metabolic oscillations in pancreatic  $\beta$ -cells, *Front. Physiol.* **12**, 781581 (2021).
- [58] M. J. Merrins, C. Poudel, J. P. McKenna, J. Ha, A. Sherman, R. Bertram, and L. S. Satin, Phase analysis of metabolic oscillations and membrane potential in pancreatic islet  $\beta$ -cells, *Biophys. J.* **110**, 691 (2016).
- [59] L. Chrobok, M. D. C. Belle, and J. Myung, From fast oscillations to circadian rhythms: Coupling at multiscale frequency bands in the rodent subcortical visual system, *Front. Physiol.* **12**, 738229 (2021).
- [60] S. Makovkin, E. Kozinov, M. Ivanchenko, and S. Gordleeva, Controlling synchronization of gamma oscillations by astrocytic modulation in a model hippocampal neural network, *Sci. Rep.* **12**, 6970 (2022).
- [61] H. Bi, M. Segneri, M. Di Volo, and A. Torcini, Coexistence of fast and slow gamma oscillations in one population of inhibitory spiking neurons, *Phys. Rev. Res.* **2**, 013042 (2020).
- [62] L. S. Satin, P. C. Butler, J. Ha, and A. S. Sherman, Pulsatile insulin secretion, impaired glucose tolerance and type 2 diabetes, *Mol. Aspects Med.* **42**, 61 (2015).
- [63] J. J. Palop and L. Mucke, Amyloid- $\beta$ -induced neuronal dysfunction in Alzheimer's disease: From synapses toward neural networks, *Nat. Neurosci.* **13**, 812 (2010).
- [64] F. Roselli and P. Caroni, Perspective from intrinsic firing properties to selective neuronal vulnerability in neurodegenerative diseases, *Neuron* **85**, 901 (2015).
- [65] V. Nimmrich, A. Draguhn, and N. Axmacher, Neuronal network oscillations in neurodegenerative diseases, *Neuromolecular Med.* **17**, 270 (2015).
- [66] B. Van Zundert, P. Izaurieta, E. Fritz, and F. J. Alvarez, Early pathogenesis in the adult-onset neurodegenerative disease amyotrophic lateral sclerosis, *J. Cell. Biochem.* **113**, 3301 (2012).